




## Curvature-induced repulsive effect on the lateral Casimir-Polder–van der Waals force

Danilo T. Alves <sup>1,2,\*</sup>, Lucas Queiroz <sup>1,†</sup>, Edson C. M. Nogueira <sup>1,‡</sup> and N. M. R. Peres<sup>2,3,§</sup>

<sup>1</sup>*Faculdade de Física, Universidade Federal do Pará, 66075-110, Belém, Pará, Brazil*

<sup>2</sup>*Centro de Física, Universidade do Minho, P-4710-057, Braga, Portugal*

<sup>3</sup>*Departamento de Física, Universidade do Minho, P-4710-057, Braga, Portugal*



(Received 17 August 2022; revised 11 April 2023; accepted 13 June 2023; published 27 June 2023)

Recently, it was shown that when a single protuberance is introduced on an infinite flat conducting surface, an anisotropic particle, kept constrained to move on a plane above the surface, can feel not only a lateral van der Waals (vdW) force that leads it to the protuberance, but, when the protuberance is narrow enough, a lateral force that moves it away from the protuberance. Although this sign inversion in the lateral vdW force was found to be related to the increasing in the curvature of the protuberance, the role of the curvature was not directly isolated from the effect caused by the remaining infinite planar surface. In this paper, seeking to isolate the sign inversion of the lateral vdW force as a result of the increase in curvature of an object, we consider a perfectly conducting infinite cylinder and investigate the vdW interaction with a neutral polarizable point particle constrained to move in a plane near the cylinder. We show that, under the action of the lateral vdW force, an isotropic polarizable particle is always attracted to the point on the plane which is closest to the cylinder surface. On the other hand, when we have an anisotropic particle, for certain particle orientations, anisotropy, and sufficiently high curvature of the cylinder, this lateral vdW force can manifest a repulsive behavior, moving the particle away from the cylinder. Since, in the literature, the sign inversion in the lateral force was discussed only in the context of the vdW regime, here we also extend this inversion to the Casimir-Polder regime. In addition, we also show that there are classical counterparts of this sign inversion effect, involving a neutral point particle with a permanent electric dipole moment.

DOI: [10.1103/PhysRevA.107.062821](https://doi.org/10.1103/PhysRevA.107.062821)

### I. INTRODUCTION

The quantum electromagnetic dispersive force between a polarizable particle and a macroscopic body is, generally, denominated as the Casimir-Polder (CP) force, or as van der Waals (vdW) force in the nonretarded regime [1–6]. Their attractive or repulsive character can be influenced, for instance, by the particle anisotropy and geometry of the bodies [7–11]. For example, an anisotropic polarizable particle can feel a normal repulsive force when it is put on the symmetry axis of a thin metal plate with a hole [7] or of a perfectly conducting toroid [8]. In both cases, for a finite distance from the particle to the origin, as we increase the radius of the hole (or toroid), from a certain value of the radius the repulsion effect can occur.

When corrugations are considered on the surface, lateral CP–vdW forces appear, and nontrivial geometric effects can be predicted, especially for these particular components of these forces [11–25]. For instance, in Ref. [22], it was shown that, when a sinusoidal corrugation with period  $L$  is introduced on an infinite flat conducting surface at  $x = 0$ , an anisotropic particle, kept constrained to move on a plane  $x = x_0$  above the

surface, feels a lateral vdW force that leads it to the nearest corrugation peak when sufficiently small values of the ratio  $x_0/L$  are considered. Otherwise, increasing the ratio  $x_0/L$ , the lateral vdW force can change its sign, moving the particle away from the corrugation peak [22]. In Ref. [24], it was considered a flat surface, still infinite, with only a single slight protuberance. In this case, it was shown that a sign inversion in the lateral vdW force can still occur when the protuberance is narrowed [the ratio  $x_0/l$  increases, with  $l$  being the characteristic width of the protuberance as shown in Fig. 1(a)]. On the other hand, the increasing curvature of the protuberance [its narrowing in the  $y$  direction, as illustrated from Fig. 1(a)(i) to 1(a)(ii)] changes not only the induced charges on it but those on the plane (since the charge distribution on the protuberance and that on the remaining infinite plane affect each other). Thus, on the sign inversion in the lateral vdW force, this model did not allow a direct isolation of the role of the increasing curvature of the protuberance from the effect caused by the remaining infinite planar surface.

In this paper, seeking to isolate the sign inversion of the lateral force as a result of the increase in curvature of an object, we consider a conducting cylinder with its symmetry axis in the  $z$  direction, as shown in Fig. 1(b), and investigate the occurrence of a similar sign inversion in the lateral vdW force. Our initial conjecture (which will be confirmed along this paper) is that a neutral anisotropic polarizable point particle, kept constrained to move on a given plane distant  $x_0 > R$  from the cylinder axis (with  $R$  being the cylinder radius), could

\*danilo@ufpa.br

†lucas.silva@icen.ufpa.br

‡edson.moraes.nogueira@icen.ufpa.br

§peres1975@gmail.com

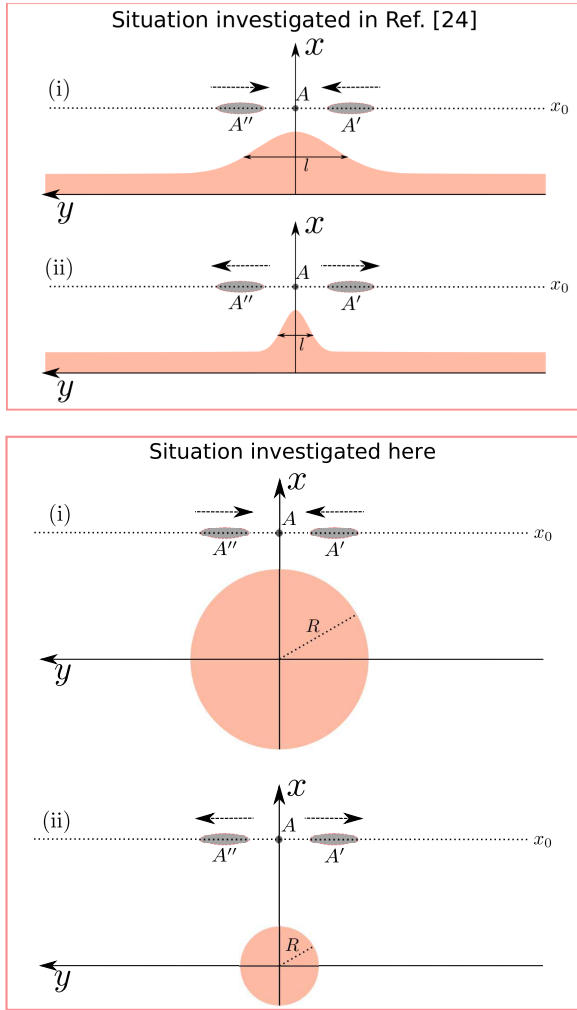


FIG. 1. Illustration of the lateral force (arrows) acting on a neutral anisotropic polarizable particle (elliptic figures), kept constrained to move on a given plane  $x = x_0$  (horizontal dotted lines), in the presence a perfectly reflecting surface. In (a), we illustrate the case of a single protuberance, with characteristic width  $l$ : in (a)(i), the particle feels a lateral force  $F^{(y)}$  taking it back to  $A$ ; in (a)(ii), for an increased ratio  $x_0/l$ ,  $F^{(y)}$  moves the particle away from  $A$  (this sign inversion in the lateral force was predicted in Ref. [24]). In (b), we illustrate our initial conjecture, which is investigated (and confirmed) in this paper: the sign inversion in the lateral force for an infinite cylinder of radius  $R$ , in both retarded and nonretarded regimes, as the normalized curvature increases. In (b)(i), the particle feels a lateral force  $F_{\text{CP-vdW}}^{(y)}$  that takes it back to  $A$ , which is the point on the plane closest to the cylinder surface. In (b)(ii), for an increased normalized curvature  $x_0/R$ ,  $F_{\text{CP-vdW}}^{(y)}$  moves the particle away from  $A$ , or from the cylinder. This repulsive behavior reveals a nontrivial dependence of the CP–vdW interaction on the cylinder normalized curvature.

feel a lateral vdW force that takes it back to the point closest to the cylinder when it is slightly dislocated from this point [see Fig. 1(b)(i)]. On the other hand, for sufficiently large values of the normalized curvature  $x_0/R$  [or  $1/(R/x_0)$ , where  $R/x_0$  is the normalized radius], the lateral vdW force would change its sign, moving the particle away from the cylinder [see Fig. 1(b)(ii)]. This means that, for a fixed distance  $x_0 > R$ , as we increase the ratio  $x_0/R$ , from a certain value of this ratio

one can have the appearance of such repulsive effect, which resembles the appearance of the repulsive effects shown in Refs. [7,8], as discussed above. In addition, since the sign inversion in the lateral force was discussed in the literature only in the context of the vdW (nonretarded) regime, here we also extend this inversion to the CP (retarded) regime. We consider, as done in Refs. [26–28], a perfectly reflecting surface since this allows us to write simpler formulas, which provides a quick estimate of the existence of the mentioned sign inversion in the lateral force.

The cylindrical geometry has been considered in problems involving dispersive interactions [26–34], with curvature effects discussed, for example, in Ref. [34]. In addition, the problem of how to probe geometric effects on the quantum vacuum fluctuations, by considering the lateral CP force, has been addressed [12,13]. Thus, the investigation carried out here, by predicting a curvature-induced repulsive effect on the lateral CP–vdW force, may be relevant for a better controlling of the interaction between a particle and a curved surface, as well as an additional way to understand geometric effects on the quantum vacuum fluctuations.

The paper is organized as follows. In Sec. II, we investigate the CP–vdW interaction between a perfectly reflecting infinite cylinder and a neutral polarizable particle, kept constrained to move on a given plane near the cylinder. We also discuss the classical interaction involving a neutral particle with a permanent electric dipole moment. In Sec. V we discuss some implications of our results, and present our final comments.

## II. CASIMIR-POLDER–VAN DER WAALS INTERACTION

### A. Casimir-Polder regime

Let us start by considering the retarded (CP) regime, and investigate the quantum energy interaction  $U_{\text{CP}}$  between a perfectly reflecting infinite cylinder and a neutral polarizable point particle located at  $(x_0, y_0, z_0)$ , oriented in space in such a way that its principal axes are parallel to the  $xyz$  axes of a Cartesian system, as illustrated in Fig. 2. In this way, an electric field applied on the particle, along any one of these Cartesian axes, induces a dipole moment in the same direction [35]. Although this is a particular orientation of a polarizable point particle in space, it is sufficient to reveal the curvature-induced repulsive effect on the lateral CP–vdW force, which is the main focus of this paper. We remark that, for an anisotropic polarizable particle (such anisotropy can be related to its geometry), the magnitude of this induced dipole moment is different in each direction and, because of this, we illustrate this particle throughout the paper as being elongated (although we are considering point particles), where the direction of such elongation is that in which the particle has the greatest polarizability. We also consider this particle characterized by a frequency-dependent polarizability tensor  $\overleftrightarrow{\alpha}(\omega)$ , whose representation  $\alpha^{(\text{cart})}(\omega)$  in the Cartesian system is given by

$$\alpha^{(\text{cart})}(\omega) = \begin{bmatrix} \alpha_{xx}(\omega) & 0 & 0 \\ 0 & \alpha_{yy}(\omega) & 0 \\ 0 & 0 & \alpha_{zz}(\omega) \end{bmatrix}. \quad (1)$$

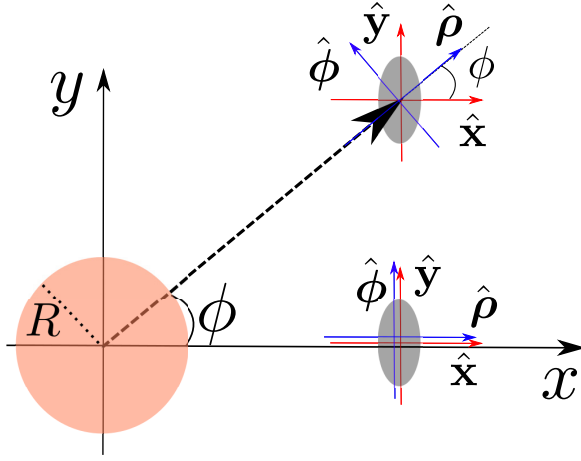


FIG. 2. Illustration of a conducting cylinder, a neutral polarizable particle (shown in two positions), and the Cartesian system  $xyz$  ( $z$  axis is perpendicular to the paper plane). The particle is oriented in space in such a way that its principal axes are parallel to the  $xyz$  axes. In one position of the particle, for which  $\phi = 0$ , these principal axes coincide with the cylindrical ones. When the particle is translated to another position for which  $\phi \neq 0$ , these axes do not coincide anymore.

The tensor  $\overleftrightarrow{\alpha}(\omega)$ , for a translated particle as illustrated in Fig. 2, is represented in cylindrical coordinate system  $(\rho, \phi, z)$  by means of the matrix  $\alpha^{(\text{cil})}(\omega, \phi)$  given by

$$\alpha^{(\text{cil})}(\omega, \phi) = \begin{bmatrix} \alpha_{\rho\rho}(\omega, \phi) & \alpha_{\rho\phi}(\omega, \phi) & 0 \\ \alpha_{\phi\rho}(\omega, \phi) & \alpha_{\phi\phi}(\omega, \phi) & 0 \\ 0 & 0 & \alpha_{zz}(\omega) \end{bmatrix}, \quad (2)$$

where  $\alpha_{\rho\rho}(\omega, \phi) = \alpha_{yy}(\omega) \sin^2 \phi + \alpha_{xx}(\omega) \cos^2 \phi$ ,  $\alpha_{\rho\phi}(\omega, \phi) = \alpha_{\phi\rho}(\omega, \phi) = [\alpha_{yy}(\omega) - \alpha_{xx}(\omega)] \sin \phi \cos \phi$ ,  $\alpha_{\phi\phi}(\omega, \phi) = \alpha_{yy}(\omega) \cos^2 \phi + \alpha_{xx}(\omega) \sin^2 \phi$ . Note that  $\alpha^{(\text{cart})}(\omega) = \alpha^{(\text{cil})}(\omega, 0)$ ,  $\cos \phi = x/\rho$ , and  $\sin \phi = y/\rho$ .

To investigate the behavior of the interaction between the particle and the cylinder, we take into account Eqs. (17) and (27)–(29) from Ref. [27], which were found considering the lowest nonvanishing order of perturbation theory and the electric-dipole approximation, as shown in the Appendix (the same formulas were also obtained in Ref. [28] by means of the Green's tensor method). In the CP interaction, one has  $\lambda_{ji} \ll \delta$ , with  $\delta = \sqrt{x_0^2 + y_0^2} - R$  and  $\lambda_{ji}$  being, respectively, the distance of the particle from the cylinder, and the wavelength of a typical transition between the states  $i$  and  $j$  of the particle [27]. Thus, the behavior of  $U_{\text{CP}}$  can be investigated by considering, in the mentioned Eqs. (17) and (27)–(29) of Ref. [27], the limit  $\lambda_{ji} \rightarrow 0$  (or  $E_{ji} \rightarrow \infty$ , since  $\lambda_{ji} \propto 1/E_{ji}$ , with  $E_{ji}$  being the energy of the transition between the states  $i$  and  $j$ ). The obtained formula can be written in terms of the static polarizability tensor  $\overleftrightarrow{\alpha}(0)$ , specifically of the diagonal components  $\rho\rho$ ,  $\phi\phi$ , and  $zz$ , which are given by

$$\alpha_{kk}(0) = \sum_{j \neq i} \frac{2| \langle j | \hat{d}_k | i \rangle |^2}{E_{ji}}, \quad (3)$$

where  $\hat{d}_k$  ( $k = \rho, \phi, z$ ) are the components of the dipole moment operator. For a translated particle (see Fig. 2),

these components depend on  $\phi$  according to Eq. (2), so that we use  $\alpha_{\rho\rho}(0, \phi) = \alpha_{xx}(0)x^2/\rho^2 + \alpha_{yy}(0)y^2/\rho^2$ , and  $\alpha_{\phi\phi}(0, \phi) = \alpha_{xx}(0)y^2/\rho^2 + \alpha_{yy}(0)x^2/\rho^2$  in the obtained formula. Thus, one has

$$U_{\text{CP}}(\bar{x}, \bar{y}) = -\frac{\hbar c}{(4\pi)^2 \epsilon_0 R^4} \left[ \Xi_{\rho}^{(\text{CP})}(\bar{\rho}) \left( \alpha_{xx}(0) \frac{\bar{x}^2}{\bar{\rho}^2} + \alpha_{yy}(0) \frac{\bar{y}^2}{\bar{\rho}^2} \right) + \Xi_{\phi}^{(\text{CP})}(\bar{\rho}) \left( \alpha_{xx}(0) \frac{\bar{y}^2}{\bar{\rho}^2} + \alpha_{yy}(0) \frac{\bar{x}^2}{\bar{\rho}^2} \right) + \Xi_z^{(\text{CP})}(\bar{\rho}) \alpha_{zz}(0) \right], \quad (4)$$

where

$$\Xi_{\rho}^{(\text{CP})}(\bar{\rho}) = 2 \sum_{m=0}^{\infty} \int_0^{\infty} du u \left\{ u^2 \frac{I_m(u)}{K_m(u)} [K'_m(u\bar{\rho})]^2 - \frac{m^2}{\bar{\rho}^2} \frac{I'_m(u)}{K'_m(u)} [K_m(u\bar{\rho})]^2 \right\}, \quad (5)$$

$$\Xi_{\phi}^{(\text{CP})}(\bar{\rho}) = 2 \sum_{m=0}^{\infty} \int_0^{\infty} du u \left\{ -u^2 \frac{I'_m(u)}{K'_m(u)} [K'_m(u\bar{\rho})]^2 + \frac{m^2}{\bar{\rho}^2} \frac{I_m(u)}{K_m(u)} [K_m(u\bar{\rho})]^2 \right\}, \quad (6)$$

$$\Xi_z^{(\text{CP})}(\bar{\rho}) = 4 \sum_{m=0}^{\infty} \int_0^{\infty} du u^3 \frac{I_m(u)}{K_m(u)} [K_m(u\bar{\rho})]^2, \quad (7)$$

where  $I_m$  and  $K_m$  are modified Bessel functions of first and second kind, respectively, and  $\sum_{m=0}^{\infty} f_m = \frac{1}{2}f_0 + \sum_{m=1}^{\infty} f_m$ ,  $R$  being the cylinder radius,  $\bar{x} = x/R$ ,  $\bar{y} = y/R$ ,  $\bar{\rho} = \rho/R$ . We highlight that once the particle is located at a distance  $\delta \gg \lambda_{ji}$ , the limit  $\lambda_{ji} \rightarrow 0$  can be applied in Eqs. (17) and (27)–(29) of Ref. [27], with such application being independent of the value of  $R$ . In other words, the retardation effects will be relevant depending only on the relation between  $\delta$  and  $\lambda_{ji}$ , and are not affected by the thickness of the cylinder with respect to  $\lambda_{ji}$  [27].

We start our analysis with the idealized case in which  $\alpha_{xx}(0) = \alpha_{zz}(0) = 0$ . Now, let us keep the particle constrained to move on a given plane  $\bar{x} = \bar{x}_0 > 1$  (see Fig. 2). We remark that such constraint, also considered in Refs. [22–25], is just a way to neutralize the action of the  $x$  component (normal) of the force, enabling us to focus only on the behavior of the  $y$  component (lateral).

From Eq. (4), we have that  $\partial U_{\text{CP}}/\partial y = 0$  along the dashed and dotted-dashed lines shown in Fig. 3, with  $[\partial^2 U_{\text{CP}}(x_0, y)/\partial y^2] > 0$  [minimum points of  $U_{\text{CP}}(x_0, y)$ ] along the dashed line, and  $[\partial^2 U_{\text{CP}}(x_0, y)/\partial y^2] < 0$  [maximum points of  $U_{\text{CP}}(x_0, y)$ ] along the dotted-dashed one. Thus, in Fig. 3, a particle in the dark region ( $1 < \bar{x} < 6.44$ ), slightly dislocated from a point in the plane  $y = 0$ , feels a force  $\mathbf{F}_{\text{CP}}^{(y)} = -\partial U_{\text{CP}}(x_0, y)/\partial y \hat{y}$  that takes it back to  $y = 0$ . On the other hand, in the light region ( $6.44 < \bar{x}$ ), the particle is moved away from  $y = 0$  or, in other words, away from the cylinder (see Fig. 3). This sign inversion in  $\mathbf{F}_{\text{CP}}^{(y)}$ , changing from an attractive character to a repulsive one, is a nontrivial geometric

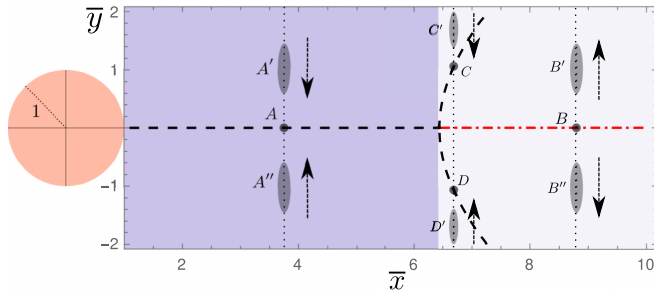


FIG. 3. Some features of the CP interaction between a perfectly reflecting cylinder and a polarizable particle (illustrated in several positions by the ellipsoidal figures), with  $\alpha_{xx}(0) = \alpha_{zz}(0) = 0$ , and kept constrained to move on a given plane  $\bar{x} = \bar{x}_0 > 1$  (three of them represented by the vertical dotted lines). Note that the cylinder circular section and the axes  $\bar{x}$  and  $\bar{y}$  are represented at a same scale. We also remark that the dashed and dotted-dashed lines are plotted taking into account Eq. (4). We have  $\partial U_{CP}/\partial y = 0$  on both dashed and dotted-dashed lines, with the dashed line corresponding to minimum points of  $U_{CP}(x_0, y)$ , whereas the dotted-dashed one corresponding to maximum points. In the dark region ( $1 < \bar{x} < 6.44$ ), when the particle is dislocated, along the  $y$  axis, for instance, from the point  $A$  to  $A'$  (or  $A''$ ), it feels a force  $\mathbf{F}_{CP}^{(y)}$  (represented by the arrows) which takes it back to  $A$ . In the light region ( $6.44 < \bar{x}$ ), when the particle is dislocated, for instance, from the point  $B$  to  $B'$  (or  $B''$ ), it feels a force  $\mathbf{F}_{CP}^{(y)}$  which moves it away from  $B$ , and, consequently, away from the cylinder. This sign inversion in  $\mathbf{F}_{CP}^{(y)}$  is a nontrivial geometric effect regulated by the normalized curvature  $\bar{x} = x/R$ . When the particle is dislocated, along  $\bar{x} = \bar{x}_0$ , for instance, from the point  $C$  to  $C'$  (or from  $D$  to  $D'$ ), it feels a force  $\mathbf{F}_{CP}^{(x)}$  that moves it back to  $C$  ( $D$ ).

effect regulated by the normalized curvature  $\bar{x}$ . The behavior of  $U_{CP}(\bar{x}_0, \bar{y})$ , for some values of  $\bar{x}_0$ , is shown in Fig. 4. In this figure, when comparing Figs. 4(a) (attractive lateral force) and 4(d) (repulsive lateral force), one notes that the magnitude of the energy remains in the same order, and, thus, the magnitude of the lateral force in these situations also has the same order.

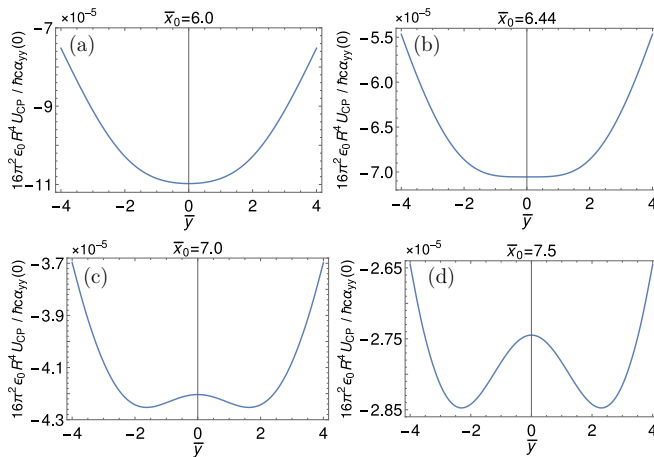


FIG. 4. The behavior of  $U_{CP}(\bar{x}_0, \bar{y})$  for some values of  $\bar{x}_0$ . In (a),  $\bar{x}_0 = 6.00$ . In (b),  $\bar{x}_0 = 6.44$ . In (c),  $\bar{x}_0 = 7.00$ . In (d),  $\bar{x}_0 = 7.50$ . (a), (b) Correspond to the dark region in Fig. 3, whereas (c) and (d) to the light one.

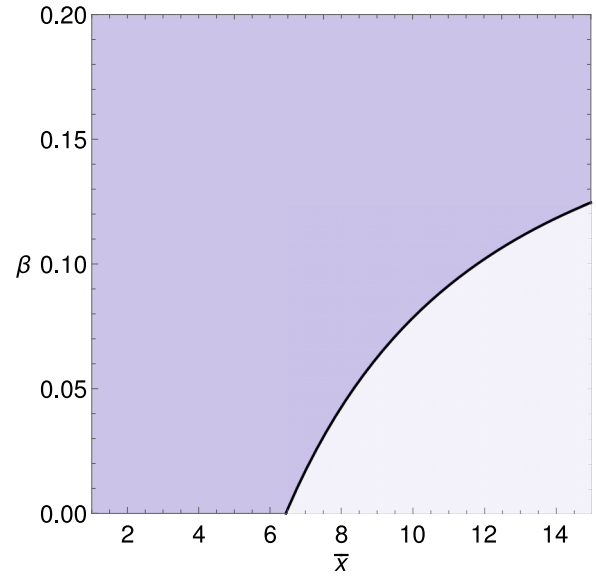


FIG. 5. For a particle characterized by  $\alpha_{xx}(0) = \alpha_{zz}(0) = \beta\alpha_{yy}(0)$ , it is shown the configurations of  $\beta$  and  $\bar{x}$  for which  $y = 0$  is a minimum (dark region) or a maximum (light region) point of  $U_{CP}(x_0, y)$ . The border between these two regions is given by the curve  $\bar{x} = \gamma(\beta)$ . We remark that  $\gamma(0) \approx 6.44$  (the situation discussed in Fig. 3), and that above  $\beta \approx 0.2$  we just have a dark region.

For a particle with  $\alpha_{xx}(0) = \alpha_{zz}(0) = \beta\alpha_{yy}(0)$ , with  $0 \leq \beta < 0.2$ , we have a behavior similar to that shown in Fig. 3, but with the border between the dark and light regions occurring at a value  $\bar{x} = \gamma(\beta)$ . In Fig. 5, we show the configurations of  $\beta$  and  $\bar{x}$  for which  $y = 0$  is a minimum (dark region) or a maximum (light region) point of  $U_{CP}(x_0, y)$ . Thus, the dark region of this figure represents configurations for which  $[\partial^2 U_{CP}(x_0, y)/\partial y^2]_{y=0} > 0$ , and the behavior of the lateral force is similar to that described for the dark region in Fig. 3. Aside from this, the light region represents  $[\partial^2 U_{CP}(x_0, y)/\partial y^2]_{y=0} < 0$ , and the behavior is similar to that described for the light region in Fig. 3. The border between the two regions in Fig. 5 is given by the curve  $\bar{x} = \gamma(\beta)$ . Note that  $\gamma(0) \approx 6.44$ , which corresponds to the situation discussed in Fig. 3. We remark that for  $\beta \gtrsim 0.2$  we just have a dark region, so that any repulsive effect of the lateral force is suppressed. Isotropic polarizable particles are characterized by  $\beta = 1$  and, thus, under the action of the lateral force, these particles are always attracted to the cylinder. This means that the existence of these discussed repulsive effects demands anisotropy on the polarizability of the considered particle.

Three limiting cases can be investigated in the CP regime, namely,  $\lambda_{ji} \ll \delta \ll R$ ,  $\lambda_{ji} \ll R \ll \delta$ , and  $R \ll \lambda_{ji} \ll \delta$  [27]. When  $\lambda_{ji} \ll \delta \ll R$ , the cylinder is very large with respect to the distance from the particle to the cylinder, and thus  $R \rightarrow \infty$  can be considered in Eqs. (5)–(7). As a consequence of this limit, the lateral force is suppressed and one recovers the original result calculated by Casimir and Polder in Ref. [4] for the retarded interaction between a particle and a perfectly conducting plane surface. In the other two cases,  $\lambda_{ji} \ll R \ll \delta$  and  $R \ll \lambda_{ji} \ll \delta$ , the cylinder is very thin with respect to the distance from the particle to the cylinder. As a consequence,



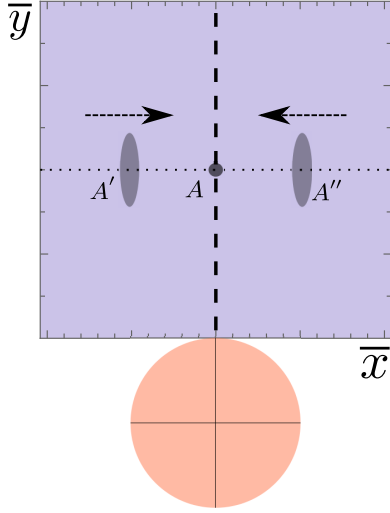


FIG. 6. Illustration of some features of the vdW-CP interaction between a perfectly reflecting cylinder and a polarizable particle (represented in two positions by the ellipsoidal figures), kept constrained to move on a given plane  $\bar{y} = \bar{y}_0 > 1$  (represented by the dotted line). The dashed line corresponds to minimum points of  $U_{\text{CP-vdW}}(x, y_0)$ , so that when the particle is dislocated, for instance, from the point A to A' (or A''), it feels a force  $\mathbf{F}_{\text{CP-vdW}}^{(x)}$  (represented by the arrows) which takes it back to A.

the greatest contributions for the summations in Eqs. (5)–(7) come from the lowest values of  $m$  [27], so that, when we consider them up to  $m = 1$ , one has

$$\begin{aligned} \Xi_{\rho}^{(\text{CP})}(\bar{\rho}) &\approx \int_0^{\infty} du u \left[ u^2 \frac{I_0(u)}{K_0(u)} - \frac{2}{\bar{\rho}^2} \frac{I_1'(u)}{K_1'(u)} [K_1(u\bar{\rho})]^2 \right. \\ &\quad \left. + 2 \int_0^{\infty} du u^3 \frac{I_1(u)}{K_1(u)} [K_1'(u\bar{\rho})]^2, \right. \end{aligned} \quad (8)$$

$$\begin{aligned} \Xi_{\phi}^{(\text{CP})}(\bar{\rho}) &\approx \int_0^{\infty} du u \left( u^2 + \frac{2}{\bar{\rho}^2} \right) \frac{I_1(u)}{K_1(u)} [K_1(u\bar{\rho})]^2 \\ &\quad - 2 \int_0^{\infty} du u^3 \frac{I_1'(u)}{K_1'(u)} [K_1'(u\bar{\rho})]^2, \end{aligned} \quad (9)$$

$$\begin{aligned} \Xi_z^{(\text{CP})}(\bar{\rho}) &\approx 2 \int_0^{\infty} du u^3 \left\{ \frac{I_0(u)}{K_0(u)} [K_0(u\bar{\rho})]^2 \right. \\ &\quad \left. + 2 \frac{I_1(u)}{K_1(u)} [K_1(u\bar{\rho})]^2 \right\}. \end{aligned} \quad (10)$$

Since these equations were obtained considering  $R \ll \delta$ , they give a better description of the CP interaction for particles in the light region in Fig. 3 (where the repulsive effect in the lateral force occurs) than in the dark one.

It is worth to mention that these curvature-induced effects are affected by the particle orientation in relation to the plane where it is kept constrained to move. As an example, let us consider the particle with  $\alpha_{xx}(0) = \alpha_{zz}(0) = \beta\alpha_{yy}(0)$  ( $0 \leq \beta \leq 1$ ) oriented as illustrated in Fig. 2, and kept constrained to move on a given plane  $y = y_0 > 1$  (see Fig. 6). In this case, we have that the point  $x = 0$  is always a minimum point of  $U_{\text{CP}}(x, y_0)$ , independent on the value of  $\beta$  or  $\bar{y}$ . This means that, when this particle is slightly dislocated from a point in

the plane  $x = 0$ , it feels a force  $\mathbf{F}_{\text{CP}}^{(x)} = -\partial U_{\text{CP}}(x, y_0)/\partial x \hat{x}$  that takes it back to  $x = 0$  in all values of  $\bar{y}$  (see Fig. 6).

## B. The van der Waals regime

Now, let us consider the nonretarded (vdW) regime, and investigate the quantum energy interaction  $U_{\text{vdW}}$ . In this regime, one has  $\delta \ll \lambda_{ji}$ , and thus, the behavior of  $U_{\text{vdW}}$  can be investigated by considering, in Eqs. (17) and (27)–(29) of Ref. [27], the limit  $\lambda_{ji} \rightarrow \infty$  (or  $E_{ji} \rightarrow 0$ ). After this, one obtains the formula for  $U_{\text{vdW}}$  given by Eq. (19) in Ref. [26], which is written in terms of the expectation values  $\langle \hat{d}_{\rho}^2 \rangle$ ,  $\langle \hat{d}_{\phi}^2 \rangle$ , and  $\langle \hat{d}_z^2 \rangle$ . For a translated particle (see Fig. 2), the components  $\alpha_{\rho\rho}$  and  $\alpha_{\phi\phi}$  depend on  $\phi$  according to Eq. (2), so that we write  $\langle \hat{d}_{\rho}^2 \rangle(\phi) = \frac{\hbar}{\pi} \int_0^{\infty} d\xi \alpha_{\rho\rho}(i\xi, \phi) = \langle \hat{d}_x^2 \rangle x^2/\rho^2 + \langle \hat{d}_y^2 \rangle y^2/\rho^2$ , and  $\langle \hat{d}_{\phi}^2 \rangle(\phi) = \frac{\hbar}{\pi} \int_0^{\infty} d\xi \alpha_{\phi\phi}(i\xi, \phi) = \langle \hat{d}_x^2 \rangle y^2/\rho^2 + \langle \hat{d}_y^2 \rangle x^2/\rho^2$ . Thus, one obtains

$$\begin{aligned} U_{\text{vdW}}(\bar{x}, \bar{y}) &= -\frac{1}{4\pi\epsilon_0 R^3} \left[ \Xi_{\rho}^{(\text{vdW})}(\bar{\rho}) \left( \langle \hat{d}_x^2 \rangle \frac{\bar{x}^2}{\bar{\rho}^2} + \langle \hat{d}_y^2 \rangle \frac{\bar{y}^2}{\bar{\rho}^2} \right) \right. \\ &\quad \left. + \Xi_{\phi}^{(\text{vdW})}(\bar{\rho}) \left( \langle \hat{d}_x^2 \rangle \frac{\bar{y}^2}{\bar{\rho}^2} + \langle \hat{d}_y^2 \rangle \frac{\bar{x}^2}{\bar{\rho}^2} \right) \right. \\ &\quad \left. + \Xi_z^{(\text{vdW})}(\bar{\rho}) \langle \hat{d}_z^2 \rangle \right], \end{aligned} \quad (11)$$

where

$$\Xi_{\rho}^{(\text{vdW})}(\bar{\rho}) = \frac{2}{\pi} \sum_{m=0}^{\infty} \int_0^{\infty} du u^2 \frac{I_m(u)}{K_m(u)} [K_m'(u\bar{\rho})]^2, \quad (12)$$

$$\Xi_{\phi}^{(\text{vdW})}(\bar{\rho}) = \frac{2}{\pi} \sum_{m=1}^{\infty} \frac{m^2}{\bar{\rho}^2} \int_0^{\infty} du \frac{I_m(u)}{K_m(u)} [K_m(u\bar{\rho})]^2, \quad (13)$$

$$\Xi_z^{(\text{vdW})}(\bar{\rho}) = \frac{2}{\pi} \sum_{m=0}^{\infty} \int_0^{\infty} du u^2 \frac{I_m(u)}{K_m(u)} [K_m(u\bar{\rho})]^2, \quad (14)$$

with  $\langle \hat{d}_j^2 \rangle = \frac{\hbar}{\pi} \int_0^{\infty} d\xi \alpha_{jj}(i\xi)$ , for  $j = x, y, z$ . We highlight that, as in the CP case, the limit  $\lambda_{ji} \rightarrow \infty$  (or  $E_{ji} \rightarrow 0$ ), used to investigate the behavior of  $U_{\text{vdW}}$  [given by Eqs. (11)–(14)], can be considered independent on  $R$ , which means that the condition  $\delta \ll \lambda_{ji}$  is sufficient for the retardation effects to be neglected.

For the vdW case, we carry out an analysis similarly to that done for the CP case. We start, again, focusing on the idealized case of a particle characterized by  $\langle \hat{d}_x^2 \rangle = \langle \hat{d}_z^2 \rangle = 0$ . For a particle kept constrained to move on a given plane  $\bar{x} = \bar{x}_0 > 1$ , from Eq. (11), we have that the dashed and dotted-dashed lines shown in Fig. 7 represent the minimum and maximum points of  $U_{\text{vdW}}(\bar{x}_0, \bar{y})$ , respectively. In this figure, the division between the dark and light regions occurs at  $\bar{x} \approx 2.18$ . The behavior of  $U_{\text{vdW}}(\bar{x}_0, \bar{y})$ , for some values of  $\bar{x}_0$ , is shown in Fig. 8. When  $\bar{y} = 0$ , we have  $\bar{x} = (\delta + R)/R$ ; thus if  $\bar{x} = 1.5$  or  $\bar{x} = 3$ , one has  $\bar{\delta} = 0.5$  and  $\bar{\delta} = 2$  (with  $\bar{\delta} = \delta/R$ ), respectively. In this way, when we change the value of  $\bar{x}$  from  $\bar{x} = 1.5$  to 3, as done from Fig. 8(a) to 8(d), the distance from the particle to the surface of the cylinder quadruplicates, and this results in a difference of two orders of magnitude in the energy, with such difference being carried to the magnitude of the lateral force.

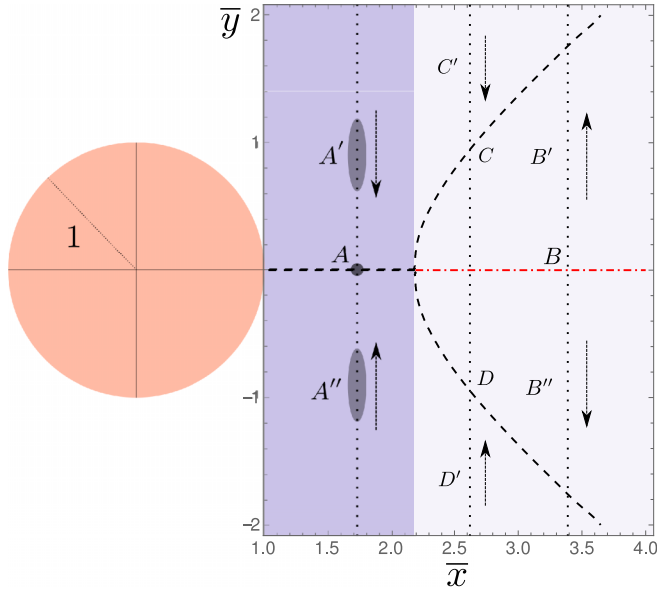


FIG. 7. Some features of the vdW interaction between a perfectly reflecting cylinder and a polarizable particle (represented in several positions by the ellipsoidal figures), with  $\langle \hat{d}_x^2 \rangle = \langle \hat{d}_z^2 \rangle = 0$ , and kept constrained to move on a given plane  $\bar{x} = \bar{x}_0 > 1$  (three of them represented by the vertical dotted lines). Note that the cylinder circular section and the axes  $\bar{x}$  and  $\bar{y}$  are represented at a same scale. We also remark that the dashed and dotted-dashed lines are plotted taking into account Eq. (11). We have  $\partial U_{\text{vdW}}/\partial y = 0$  on both dashed and dotted-dashed lines, with the dashed line corresponding to minimum points of  $U_{\text{vdW}}(x_0, y)$ , whereas the dotted-dashed one corresponding to maximum points. In dark region ( $1 < \bar{x} < 2.18$ ), when the particle is dislocated, along the  $y$  axis, for instance, from the point  $A$  to  $A'$  (or  $A''$ ), it feels a force  $\mathbf{F}_{\text{vdW}}^{(y)}$  (represented by the arrows) which takes it back to  $A$ . In light region ( $2.18 < \bar{x}$ ), when the particle is dislocated, for instance, from the point  $B$  to  $B'$  (or  $B''$ ), it feels a force  $\mathbf{F}_{\text{vdW}}^{(y)}$  which moves it away from  $B$ , and, consequently, away from the cylinder. This sign inversion in  $\mathbf{F}_{\text{vdW}}^{(y)}$  is a nontrivial geometric effect regulated by the normalized curvature  $\bar{x}$ . When the particle is dislocated, along  $\bar{x} = \bar{x}_0$ , for instance, from the point  $C$  to  $C'$  (or from  $D$  to  $D'$ ), it feels a force  $\mathbf{F}_{\text{vdW}}^{(x)}$  that moves it back to  $C$  ( $D$ ).

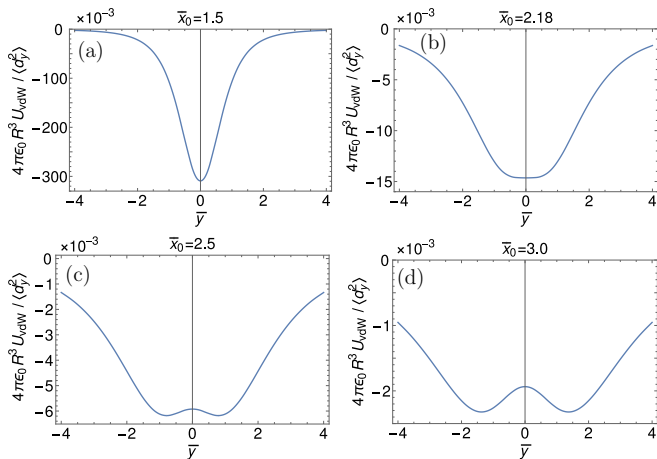


FIG. 8. The behavior of  $U_{\text{vdW}}(\bar{x}_0, \bar{y})$  for some values of  $\bar{x}_0$ . In (a),  $\bar{x}_0 = 1.50$ . In (b),  $\bar{x}_0 = 2.18$ . In (c),  $\bar{x}_0 = 2.50$ . In (d),  $\bar{x}_0 = 3.00$ . (a), (b) Correspond to the dark region in Fig. 7, whereas (c) and (d) to the light one.

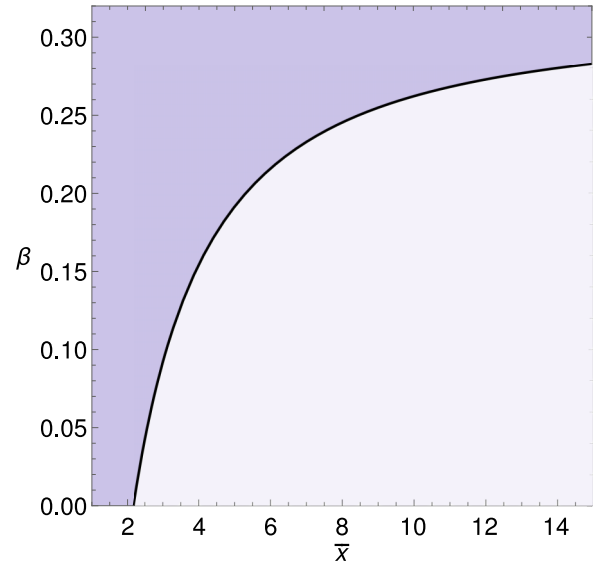


FIG. 9. For a particle characterized by  $\langle \hat{d}_x^2 \rangle = \langle \hat{d}_z^2 \rangle = \beta \langle \hat{d}_y^2 \rangle$ , it is shown the configurations of  $\beta$  and  $\bar{x}$  for which  $y = 0$  is a minimum (dark region) or a maximum (light region) point of  $U_{\text{vdW}}(x_0, y)$ . The border between these two regions is given by the curve  $\bar{x} = \gamma(\beta)$ . We remark that  $\gamma(0) \approx 2.18$  (the situation discussed in Fig. 7), and that above  $\beta \approx 0.32$  we just have a dark region.

For a particle with  $\langle \hat{d}_x^2 \rangle = \langle \hat{d}_z^2 \rangle = \beta \langle \hat{d}_y^2 \rangle$ , we show in Fig. 9 configurations of  $\beta$  and  $\bar{x}$  for which  $y = 0$  is a minimum (dark region) or a maximum (light region) point of  $U_{\text{vdW}}(x_0, y)$ . For  $\beta \gtrsim 0.32$  we just have a dark region, so that any repulsive effect of the lateral force is suppressed. Thus, as in the CP case, isotropic particles ( $\beta = 1$ ) are always attracted to the cylinder. For  $0 \leq \beta \leq 0.32$ , we can have dark and light regions, depending on  $\bar{x}$  and  $\beta$ . The border between these two regions is given by the curve  $\bar{x} = \gamma(\beta)$ . In this figure, note that  $\gamma(0) \approx 2.18$ , which corresponds to the situation discussed in Fig. 7. In summary, for a particle with  $\beta \gtrsim 0.32$  the behavior of  $F_{\text{vdW}}^{(y)}$  is given by the dark region in Fig. 7 for all  $\bar{x}$ , and only particles with  $\beta \lesssim 0.32$  can exhibit the repulsive behavior of  $F_{\text{vdW}}^{(y)}$  shown by the light region in Fig. 7. Lastly, these curvature-induced effects are affected by the particle orientation in relation to the plane where it is kept constrained to move, similar to the CP case, so that if we consider a particle oriented as illustrated in Fig. 6, we also have a force  $F_{\text{vdW}}^{(x)}$  that always take the particle to  $x = 0$ , regardless of the value of  $\bar{y}$  (see Fig. 6).

Three limiting cases can be investigated in the vdW case, namely,  $\delta \ll R \ll \lambda_{ji}$ ,  $\delta \ll \lambda_{ji} \ll R$ , and  $R \ll \delta \ll \lambda_{ji}$  [27]. In both situations  $\delta \ll R \ll \lambda_{ji}$  and  $\delta \ll \lambda_{ji} \ll R$ , the cylinder is very large with respect to the distance from the particle to the cylinder, and thus  $R \rightarrow \infty$  can be considered in Eqs. (12)–(14). As a consequence of this limit, the lateral force is suppressed and one recovers the original result for the nonretarded interaction between a particle and a perfectly conducting plane surface [36]. Now, when  $R \ll \delta \ll \lambda_{ji}$ , the cylinder is very thin with respect to the distance from the particle to the cylinder. As a consequence, the greatest contributions for the summations in Eqs. (12)–(14) come from the lowest values of  $m$  [27], so that, when considering the first

term of these summations ( $m = 0$  for  $\Xi_\rho$  and  $\Xi_z$ , and  $m = 1$  for  $\Xi_\phi$ ), one has

$$\Xi_\rho^{(\text{vdW})}(\bar{\rho}) \approx \frac{1}{\pi} \int_0^\infty du u^2 \frac{I_0(u)}{K_0(u)} [K_1(u\bar{\rho})]^2, \quad (15)$$

$$\Xi_\phi^{(\text{vdW})}(\bar{\rho}) \approx \frac{2}{\pi \bar{\rho}^2} \int_0^\infty du \frac{I_1(u)}{K_1(u)} [K_1(u\bar{\rho})]^2, \quad (16)$$

$$\Xi_z^{(\text{vdW})}(\bar{\rho}) \approx \frac{1}{\pi} \int_0^\infty du u^2 \frac{I_0(u)}{K_0(u)} [K_0(u\bar{\rho})]^2. \quad (17)$$

Since these equations were obtained considering  $R \ll \delta$  [similarly to Eqs. (8)–(10)], they give a better description of the vdW interaction for particles in the light region in Fig. 7 than in the dark one.

### III. CLASSICAL INTERACTION

The discussed curvature-induced effects have a classical counterpart, which involves the interaction between a grounded perfectly conducting infinite cylinder and a neutral point particle with an electric dipole moment vector  $\mathbf{d} = d_x \hat{\mathbf{x}} + d_y \hat{\mathbf{y}} + d_z \hat{\mathbf{z}}$ . In this situation, the interaction energy  $U_{\text{cla}}$  is simply given by replacing  $\langle \hat{d}_i^2 \rangle \rightarrow d_i^2$  in Eq. (11) [26]. In this way, one can note that the behavior of this classical interaction for the case of a particle oriented with  $d_x = d_z = 0$ , for example, is similar to the quantum one for a particle characterized by  $\langle \hat{d}_x^2 \rangle = \langle \hat{d}_z^2 \rangle = 0$ . In this situation, the dashed and dotted-dashed lines shown in Fig. 7 also represent the minimum and maximum points of  $U_{\text{cla}}(x_0, y)$ , respectively, and thus, sign inversions in the lateral force also arise in the classical context.

### IV. DISCUSSIONS

Before discussing the results presented here, it is useful to briefly review some of the ones found in Refs. [24,25] for the sign inversions in the lateral vdW forces when considering an infinite flat surface with only a slight protuberance.

A polarizable particle in the presence of a conducting plane surface feels a CP–vdW force which is normal to this plane [3,4]. On the other hand, when considering the presence of a protuberance on such plane surface, the particle can feel a force which is parallel to this plane (a lateral force). For instance, when considering a Gaussian protuberance, as illustrated in Fig. 1(a), if the particle is out of the  $x$  axis (for example, at the point  $A'$ ), beyond the force that is normal to the plane, it feels a lateral force originated in the breaking of the translation symmetry of the surface along the  $y$  axis. In Ref. [24], it was shown that while an isotropic particle feels a lateral vdW force that always tends to pull it to the protuberance, an anisotropic particle can be pulled to the protuberance as well as pushed away from it. Specifically, it was shown that increasing the curvature of the protuberance itself [its narrowing in the  $y$  direction, as illustrated from Fig. 1(a)(i) to 1(a)(ii)], a sign inversion in the lateral vdW force can occur.

The model of a single protuberance on an infinite plane did not allow to isolate the effect of the increasing curvature of the protuberance from the effect of the remaining infinite planar surface. Seeking to isolate the sign inversion of the lateral force as a result of the increase in the curvature of an object, we considered here a conducting infinite cylinder,

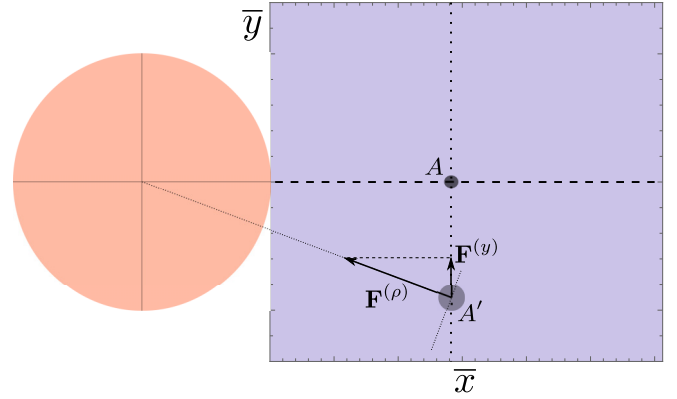


FIG. 10. Some features of the CP–vdW interaction between a perfectly reflecting cylinder and an isotropic polarizable particle (represented by the circular figure), and kept constrained to move on planes  $\bar{x} = \bar{x}_0 > 1$  (one of them represented by the vertical dotted line). The complete CP–vdW force is always radial ( $\mathbf{F} = F^{(\rho)} \hat{\rho}$ ). When the particle is dislocated along  $\bar{x} = \bar{x}_0$ , for instance, from the point  $A$  to  $A'$ , it feels a radial CP–vdW force, whose component along the  $y$  direction  $\mathbf{F}^{(y)}$  always tends to pull back the particle to  $A$ , attracting the particle to the cylinder. Thus, no sign inversion in the lateral  $\mathbf{F}^{(y)}$  occurs when the particle is isotropic.

as shown in Fig. 1(b). Note that, similar to the presence of the protuberance, the cylinder breaks the translation symmetry along the  $y$  axis, so that a particle out of the  $x$  axis, in addition to a force normal to the plane  $x = x_0$ , feels a lateral force (along the  $y$  axis), as illustrated in Fig. 1(b), whose origin is discussed next.

When considering an isotropic particle, the lateral force always attracts it to a point closest to the cylinder. This can be viewed from the fact that the complete CP–vdW force  $\mathbf{F}$  on an isotropic particle is always radial ( $\mathbf{F} = F^{(\rho)} \hat{\rho}$ ), and that its  $y$  projection,  $\mathbf{F}^{(y)} = (F^{(\rho)} \hat{\rho} \cdot \hat{\mathbf{y}}) \hat{\mathbf{y}}$ , always attracts the particle to the cylinder, as illustrated in Fig. 10.

When considering an anisotropic particle, the total CP–vdW force  $\mathbf{F}$  is not radial in general. For example, let us consider again the idealized case in which  $\alpha_{xx} = \alpha_{zz} = 0$  (see Fig. 11). When the particle is located at the point  $A$ , it feels a total CP–vdW force which is radial, but when the particle is at  $A'$ , it feels a total CP–vdW force which is no longer radial, but having a component in the  $\phi$  direction:  $\mathbf{F} = F^{(\rho)} \hat{\rho} + F^{(\phi)} \hat{\phi}$  [the existence of such a  $\phi$  component can be viewed directly from the dependence of Eqs. (4) and (11) on  $\phi$ , by means of  $\bar{x}$  and  $\bar{y}$ ]. Note that at  $A'$  the radial part of the CP–vdW force has a component in the  $y$  direction,  $\mathbf{F}^{(\rho,y)} = (F^{(\rho)} \hat{\rho} \cdot \hat{\mathbf{y}}) \hat{\mathbf{y}}$ , which pulls back the particle to the position  $A$ , whereas the  $\phi$  part has a component in the  $y$  direction,  $\mathbf{F}^{(\phi,y)} = (F^{(\phi)} \hat{\phi} \cdot \hat{\mathbf{y}}) \hat{\mathbf{y}}$ , which pushes the particle away from the position  $A$ . Thus, at  $A'$ , one has a competition between the  $y$  components from the radial and  $\phi$  parts of  $\mathbf{F}$  (see Fig. 11), so that the resultant, given by  $\mathbf{F}^{(y)} = \mathbf{F}^{(\rho,y)} + \mathbf{F}^{(\phi,y)}$ , produces an attractive behavior, pulling back the particle to the point  $A$ , or closer to the cylinder (note that this attractive behavior is because the particle is in the dark region). In contrast, when the particle is at  $B'$  (in light region),  $\mathbf{F}^{(y)}$  produces a repulsive behavior, pushing the particle away from the point  $B$  (or from the cylinder) (see Fig. 11). It is worth noting that a naive reasoning would lead to the

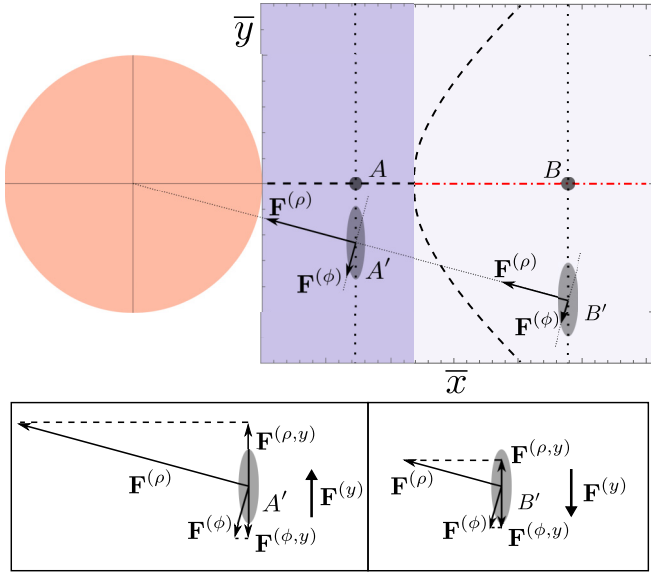


FIG. 11. Some features of the CP–vdW interaction between a perfectly reflecting cylinder and an anisotropic polarizable particle with  $\alpha_{xx} = \alpha_{zz} = 0$  (represented in some positions by ellipsoidal figures), and kept constrained to move on planes  $\bar{x} = \bar{x}_0 > 1$  (some of them represented by the vertical dotted lines). When the particle is located at a point A, it feels a total CP–vdW force  $\mathbf{F}$  which is radial. When the particle is at A',  $\mathbf{F}$  is no longer radial, having a component in the  $\phi$  direction:  $\mathbf{F} = \mathbf{F}^{(\rho)} + \mathbf{F}^{(\phi)}$ , where  $\mathbf{F}^{(\rho)} = F^{(\rho)}\hat{\rho}$  and  $\mathbf{F}^{(\phi)} = F^{(\phi)}\hat{\phi}$ . In the left inset, we illustrate the projection of  $F^{(\rho)}\hat{\rho}$  in the  $y$  direction,  $\mathbf{F}^{(\rho,y)}$ , which pulls back the particle to the position A; the projection of  $F^{(\phi)}\hat{\phi}$  in the  $y$  direction,  $\mathbf{F}^{(\phi,y)}$ , which pushes the particle away from the position A; the resultant force  $\mathbf{F}^{(y)} = \mathbf{F}^{(\rho,y)} + \mathbf{F}^{(\phi,y)}$ , producing an attractive behavior, pulling back the particle to the point A, closer to the cylinder (this attractive behavior is because the particle is in the dark region). When the particle is at B',  $\mathbf{F}$  is also not radial. In the right inset, we illustrate: the projection of  $F^{(\rho)}\hat{\rho}$  and  $F^{(\phi)}\hat{\phi}$  in the  $y$  direction; the resultant force  $\mathbf{F}^{(y)}$ , producing a repulsive behavior, pushing the particle away from the point B, or from the cylinder (this repulsive behavior is because the particle is in the light region).

expectation that, from A' to B', the magnitudes of  $\mathbf{F}^{(\rho)}$  and  $\mathbf{F}^{(\phi)}$  would decrease in the same proportion, so that  $\mathbf{F}^{(y)}$  would not change its orientation. Interestingly, this does not occur in this way, so that an imbalance in this proportion leads to a change in the orientation of  $\mathbf{F}^{(y)}$ . As shown in the previous sections, depending on the value of  $x_0/R$  (the normalized curvature),  $\mathbf{F}^{(y)}$  can result in a lateral force with an attractive character (dark region of Fig. 11) or a repulsive one, with this latter situation allowed to occur in the light region of Fig. 11.

All the above discussion focused on the action of the  $y$  component of  $\mathbf{F}$ , with the particle kept constrained to move on a given plane  $\bar{x} = \bar{x}_0 > 1$ . In this paragraph, let us remove this constraint, and also include the normal force  $\mathbf{F}^{(x)}$  in our analysis, as illustrated in Fig. 12. In the dark region, the anisotropic particle feels an attractive force  $\mathbf{F}^{(y)}$  which tends to pull back the particle to the  $x$  axis (or closer to the cylinder), and a normal force  $\mathbf{F}^{(x)}$  tending to pull the particle to the cylinder. In the light region in Fig. 12, a particle slightly dislocated from the  $x$  axis feels a repulsive force  $\mathbf{F}^{(y)}$  which

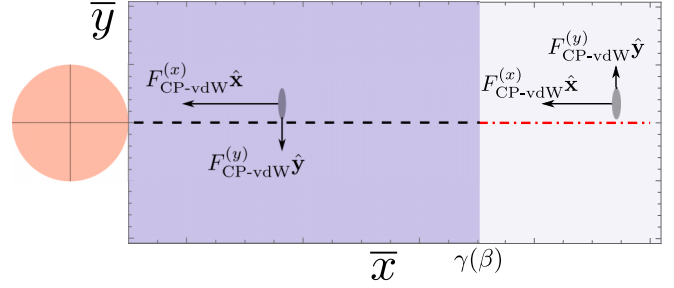


FIG. 12. Illustration of the complete CP–vdW interaction between a perfectly reflecting cylinder and a polarizable point particle (represented in two positions by the ellipsoidal figures), with  $\langle \hat{d}_x^2 \rangle = \langle \hat{d}_z^2 \rangle = 0$ . Unlike in Figs. 3 and 7, here the particle is not kept constrained to move on a given plane  $\bar{x} = \bar{x}_0 > 1$ , being free to move. In the dark region, a particle slightly dislocated from the  $x$  axis feels an attractive force  $\mathbf{F}_{\text{CP-vdW}}^{(y)}$  which tends to pull back the particle to the  $x$  axis (or closer to the cylinder), and the normal force  $\mathbf{F}_{\text{CP-vdW}}^{(x)}$  tends to pull the particle to the cylinder. In the light region, a particle slightly dislocated from the  $x$  axis feels a repulsive force  $\mathbf{F}_{\text{CP-vdW}}^{(y)}$  which tends to push the particle away from the  $x$  axis (or from the cylinder), and the normal force  $\mathbf{F}_{\text{CP-vdW}}^{(x)}$  tends to pull the particle to the cylinder.

tends to push the particle away from the  $x$  axis (or from the cylinder), and the normal force  $\mathbf{F}^{(x)}$  tending to pull the particle to the cylinder. In summary, while in the dark region both components contribute to the attraction to the cylinder, in the light region one of them ( $\mathbf{F}^{(y)}$ ) contributes to a repulsion. Thus, the repulsive behavior of  $\mathbf{F}^{(y)}$  is present, independently of the particle being constrained to move on a given plane  $\bar{x} = \bar{x}_0 > 1$ . On the other hand, this behavior can be isolated and more easily detected if such a constraint is considered, as discussed next.

The detection of such geometric effects on the lateral CP–vdW force could be done, for example, by keeping an anisotropic particle constrained to move on a given plane  $\bar{x} = \bar{x}_0 > 1$ , trapped on an external harmonic potential  $U_{\text{trap}}(y)$  with equilibrium point at  $y = 0$  (see Fig. 13), and measuring the deviation, caused by the mentioned lateral force, in the original trap frequency (see, for instance, Refs. [12,22,24,37]). Let us consider a particle with mass  $m$  and  $\alpha_{xx}(0) = \alpha_{zz}(0) = \beta\alpha_{yy}(0)$ , with  $\beta < 0.2$ , and the CP regime [or  $\langle \hat{d}_x^2 \rangle = \langle \hat{d}_z^2 \rangle = \beta\langle \hat{d}_y^2 \rangle$ , with  $\beta < 0.32$ , and the vdW regime], and oscillating with a certain frequency  $\omega_{\text{trap}}$  in the absence of the cylinder. The presence of the cylinder modifies this oscillation frequency to a new value  $\omega'_{\text{trap}} = \sqrt{\omega_{\text{trap}}^2 + m^{-1}[\partial^2 U_{\text{CP-vdW}}(x_0, y)/\partial y^2]}$ , resulting in a frequency deviation  $\delta\omega_{\text{trap}} \equiv \omega'_{\text{trap}} - \omega_{\text{trap}}$ . When  $1 < \bar{x}_0 < \gamma(\beta)$  [with  $\gamma(\beta)$  given in Figs. 5 and 9 for the CP and vdW cases, respectively], an experimental apparatus would detect  $\delta\omega_{\text{trap}} > 0$  (see dark region in Fig. 13). Otherwise, when  $\gamma(\beta) < \bar{x}_0$ , one would have  $\delta\omega_{\text{trap}} < 0$  (see light region in Fig. 13). Therefore, the sign inversion in the lateral force, changing from an attractive behavior to a repulsive one (as illustrated in Fig. 13), manifests, in this scenario, as a sign inversion in the frequency deviation  $\delta\omega_{\text{trap}}$ , with this behavior revealing a nontrivial dependence of the CP–vdW interaction with the surface geometry, specifically of the normalized curvature.



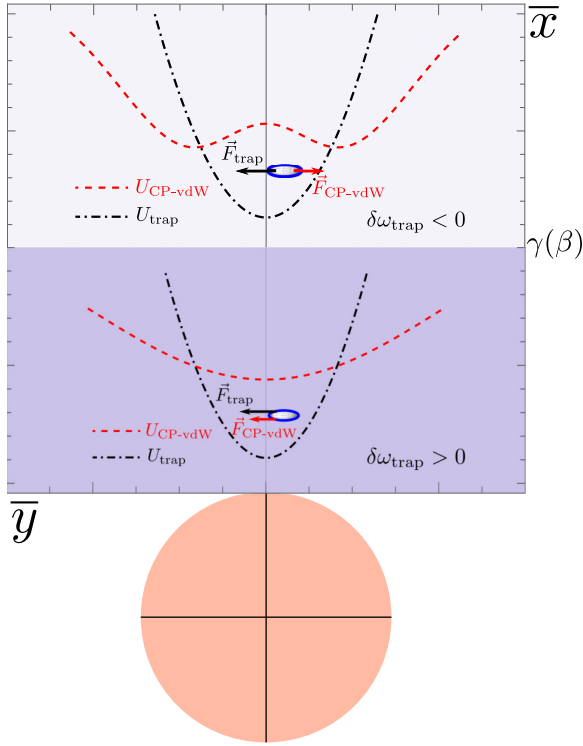


FIG. 13. Illustration of a particle kept constrained to move on a given plane  $\bar{x} = \bar{x}_0 > 1$ , and subjected to a trap harmonic potential  $U_{\text{trap}}(y)$  (illustrated by the dotted-dashed lines) with equilibrium point at  $y = 0$ , near a perfectly reflecting cylinder. The dashed lines represent  $U_{\text{CP-vdW}}(x_0, y)$ . The presence of the cylinder modifies this oscillation frequency to a new value  $\omega'_{\text{trap}}$ , resulting in a frequency deviation  $\delta\omega_{\text{trap}} \equiv \omega'_{\text{trap}} - \omega_{\text{trap}}$ . In dark region [ $1 < \bar{x} < \gamma(\beta)$ ], an experimental apparatus would detect  $\delta\omega_{\text{trap}} > 0$ . Otherwise, in light region [ $\gamma(\beta) < \bar{x}$ ], it would detect  $\delta\omega_{\text{trap}} < 0$ .

## V. FINAL REMARKS

In this paper, seeking to isolate the role of the increase in curvature of an object on the sign inversion of the lateral vdW force, the model of an infinite flat surface with a single slight protuberance [discussed in the literature [24,25] and illustrated in Fig. 1(a)] was replaced by that of a perfectly conducting infinite cylinder with radius  $R$ , as shown in Fig. 1(b). In common, both models in Figs. 1(a) and 1(b) break the translation symmetry along the  $y$  axis. On the other hand, the cylinder is a localized object in the  $y$  direction ( $-R \leq y \leq R$ ), in contrast with the infinite plane. In this way, we investigated the effect of curvature of an object on the lateral vdW force, mimicking a protuberance but removing any influence of a remaining flat surface.

We investigated the vdW interaction with a neutral polarizable point particle constrained to move in a plane distant  $x_0 > R$  from the axis of the cylinder [Fig. 1(b)]. We showed that an isotropic polarizable particle, under the action of the lateral vdW force, is always attracted to the point closest to the cylinder surface. On the other hand, when considering an anisotropic one, for certain particle orientations and anisotropy, the lateral vdW force can move it away from the cylinder (Fig. 7). In the literature, the sign inversion in the lateral force was discussed only in the context of the

vdW regime. Here, we also extended this discussion to the CP regime and found that the repulsive behavior can also occur (Fig. 3), so that we were able to make a direct connection between the sign inversion in the lateral force and the increase in curvature of an object in both vdW and CP regimes, fulfilling the main objective of this paper. Once such connection was demonstrated here in these regimes, it may be very interesting to study the behavior of such a curvature-induced repulsive behavior of the lateral force for situations of transition between these regimes, which can be done in further investigations. It would also be interesting to perform a fully electromagnetic calculation using the methods developed in Ref. [38].

Finally, we also showed that there are classical counterparts of these effects, involving a neutral point particle with a permanent electric dipole moment. The nontrivial connection between such effects and the curvature of the objects, discussed in this paper, may be relevant for a better controlling of the interaction between a particle and a curved surface in classical and quantum physics.

## ACKNOWLEDGMENTS

L.Q. and E.C.M.N. were supported by the Coordenação de Aperfeiçoamento de Pessoal de Nível Superior-Brasil (CAPES), Finance Code 001.

## APPENDIX: MAIN STEPS TO OBTAIN EQS. (4)–(7) AND (11)–(14)

In this Appendix, we briefly review the steps of the calculations performed in Ref. [27] to obtain Eqs. (4)–(7) and (11)–(14) used in this paper (in this Appendix, we consider  $\hbar = c = 1$ ). First, in Ref. [27], the authors considered the particle interacting with the quantized electromagnetic field  $\mathbf{E}$ , whose interaction Hamiltonian was given by

$$H_{\text{int}} = -\mathbf{d} \cdot \mathbf{E}, \quad (\text{A1})$$

where  $\mathbf{d}$  is the dipole moment operator. The quantized electromagnetic field was written in terms of the vector potential, which was given as a normal-mode expansion in terms of the photon annihilation and creation operators, i.e.,

$$\mathbf{A}(\mathbf{r}, t) = \sum_{\lambda, \sigma} \frac{1}{\sqrt{2\epsilon_0\omega_\lambda}} [a_\lambda^{(\sigma)} \mathbf{F}_\lambda^{(\sigma)}(\mathbf{r}) e^{-i\omega t} + \text{H.c.}], \quad (\text{A2})$$

where  $\lambda$  describes each mode of the field with polarization  $\sigma$ , and the normal modes  $\mathbf{F}(\mathbf{r})$ , in the Coulomb gauge, satisfy the vector Helmholtz equation

$$(\nabla^2 + \omega^2)\mathbf{F}(\mathbf{r}) = \mathbf{0}. \quad (\text{A3})$$

Also in Ref. [27], considering the particle in a state  $|i\rangle$  and the field in the vacuum state  $|0\rangle$ , the energy shift due to the particle-field interaction was calculated perturbatively, considering the second perturbative order (the lowest nonvanishing one), and the electric-dipole approximation, so that,

using Eqs. (A1) and (A2), the energy shift was written as

$$\Delta W = - \sum_{\lambda, \sigma, j \neq i} \frac{\omega_\lambda}{2\epsilon_0} \frac{|\langle j | \mathbf{d} | i \rangle \cdot \mathbf{F}_\lambda^{(\sigma)*}(\mathbf{r})|^2}{E_{ji} + \omega_\lambda}, \quad (\text{A4})$$

where  $E_{ji}$  is the energy of the transition between the states  $i$  and  $j$ . The matrix elements  $\langle j | \mathbf{d} | i \rangle$  are related with the particle polarizability  $\alpha_{kl}(\omega)$  as

$$\alpha_{kl}(\omega) = \sum_j \frac{2E_{ji} \langle i | \hat{d}_k | j \rangle \langle j | \hat{d}_l | i \rangle}{E_{ji}^2 - \omega^2}, \quad (\text{A5})$$

with  $\hat{d}_k$  being the components of the dipole moment operator. Thus, to obtain  $\Delta W$ , one has only to solve Eq. (A3) with the boundary condition that the tangential components of the electric field and the normal component of the magnetic field vanish at the surface of the cylinder. To calculate the interaction energy  $U(\mathbf{r}_0)$  between the particle and the conducting cylinder, the authors in Ref. [27] subtracted from Eq. (A4) the portion of the energy due to the field fluctuations in free space, so that

$$U(\mathbf{r}_0) = \Delta W - \lim_{R \rightarrow 0} \Delta W. \quad (\text{A6})$$

Therefore, the authors found that

$$U(\mathbf{r}_0) = - \frac{1}{4\pi\epsilon_0} \sum_{j \neq i} [\Xi_\rho |\hat{d}_\rho|^2 + \Xi_\phi |\hat{d}_\phi|^2 + \Xi_z |\hat{d}_z|^2] \quad (\text{A7})$$

with

$$\begin{aligned} \Xi_\rho &= \frac{2}{\pi} \sum_{m=0}^{\infty} \int_0^{\infty} dk k \\ &\times \left\{ \left( \sqrt{E_{ji}^2 + k^2} - E_{ji} \right) \frac{I_m(kR)}{K_m(kR)} [K'_m(k\rho)]^2 \right. \\ &\left. + \frac{m^2}{k^2 \rho^2} \left( \frac{E_{ji}^2}{\sqrt{E_{ji}^2 + k^2}} - E_{ji} \right) \frac{I'_m(kR)}{K'_m(kR)} [K_m(k\rho)]^2 \right\}, \end{aligned} \quad (\text{A8})$$

$$\begin{aligned} \Xi_\phi &= \frac{2}{\pi} \sum_{m=0}^{\infty} \int_0^{\infty} dk k \\ &\times \left\{ \left( \frac{E_{ji}^2}{\sqrt{E_{ji}^2 + k^2}} - E_{ji} \right) \frac{I'_m(kR)}{K'_m(kR)} [K'_m(k\rho)]^2 \right. \\ &\left. + \frac{m^2}{k^2 \rho^2} \left( \sqrt{E_{ji}^2 + k^2} - E_{ji} \right) \frac{I_m(kR)}{K_m(kR)} [K_m(k\rho)]^2 \right\}, \quad (\text{A9}) \\ \Xi_z &= \frac{2}{\pi} \sum_{m=0}^{\infty} \int_0^{\infty} dk k \left\{ \frac{k^2}{\sqrt{E_{ji}^2 + k^2}} \frac{I_m(kR)}{K_m(kR)} [K_m(k\rho)]^2 \right\}, \end{aligned} \quad (\text{A10})$$

which correspond, respectively, to Eqs. (17) and (27)–(29) of Ref. [27].

Equations (A7)–(A10) are valid to any distance  $\delta = \sqrt{x_0^2 + y_0^2} - R$  from the particle to the cylinder. In the model discussed here, the only characteristic length scale is the wavelength  $\lambda_{ji}$  (with  $\lambda_{ji} \propto 1/E_{ji}$ ) of a typical transition between the states  $i$  and  $j$  of the particle. To achieve one of the main goals of this paper, namely, to make a direct connection between the sign inversion in the lateral vdW force and the increase in curvature of an object, we consider  $\delta \ll \lambda_{ji}$ , so one makes  $\lambda_{ji} \rightarrow \infty$  (or  $E_{ji} \rightarrow 0$ ) in Eqs. (A7)–(A10). Thus, for the situation shown in Fig. 2, we obtain Eqs. (11)–(14) as describing the interaction in the vdW regime. Since, in the literature, the sign inversion in the lateral force was discussed only in the context of the vdW (nonretarded) regime, another goal of this paper is to extend this effect to the CP (retarded) regime, where  $\lambda_{ji} \ll \delta$ , and one considers the limit  $\lambda_{ji} \rightarrow 0$  (or  $E_{ji} \rightarrow \infty$ ) in Eqs. (A7)–(A10). Thus, for the situation shown in Fig. 2, we obtain Eqs. (4)–(7) as describing the interaction in the CP regime. The expressions for the interaction energies in these asymptotic limits are significantly simpler than the original general Eqs. (A7)–(A10), so that the numerical calculations needed to investigate their behavior are greatly reduced.

- 
- [1] R. Eisenschitz and F. London, Über das Verhältnis der van der Waalsschen Kräfte zu den homöopolaren Bindungskräften, *Z. Phys.* **60**, 491 (1930).
- [2] F. London, Zur theorie und systematik der molekularkräfte, *Z. Phys.* **63**, 245 (1930).
- [3] H. B. G. Casimir and D. Polder, Influence of retardation on the london–van der Waals forces, *Nature (London)* **158**, 787 (1946).
- [4] H. B. G. Casimir and D. Polder, The influence of retardation on the london–van der Waals forces, *Phys. Rev.* **73**, 360 (1948).
- [5] G. Feinberg and J. Sucher, General theory of the van der Waals interaction: A model-independent approach, *Phys. Rev. A* **2**, 2395 (1970).
- [6] V. N. Marachevsky and A. A. Sidelnikov, Green functions scattering in the casimir effect, *Universe* **7**, 195 (2021).
- [7] M. Levin, A. P. McCauley, A. W. Rodriguez, M. T. Homer Reid, and S. G. Johnson, Casimir Repulsion between Metallic Objects in Vacuum, *Phys. Rev. Lett.* **105**, 090403 (2010).
- [8] P. P. Abrantes, Y. França, F. S. S. da Rosa, C. Farina, and R. de Melo e Souza, Repulsive van der Waals interaction between a quantum particle and a conducting toroid, *Phys. Rev. A* **98**, 012511 (2018).
- [9] C. Eberlein and R. Zietal, Casimir-Polder interaction between a polarizable particle and a plate with a hole, *Phys. Rev. A* **83**, 052514 (2011).
- [10] J. J. Marchetta, P. Parashar, and K. V. Shajesh, Geometrical dependence in Casimir-Polder repulsion, *Phys. Rev. A* **104**, 032209 (2021).
- [11] S. Y. Buhmann, V. N. Marachevsky, and S. Scheel, Impact of anisotropy on the interaction of an atom with a one-dimensional nano-grating, *Int. J. Mod. Phys. A* **31**, 1641029 (2016).
- [12] D. A. R. Dalvit, P. A. Maia Neto, A. Lambrecht, and S. Reynaud, Probing Quantum-Vacuum Geometrical Effects with Cold Atoms, *Phys. Rev. Lett.* **100**, 040405 (2008).

- [13] D. A. R. Dalvit, P. A. M. Neto, A. Lambrecht, and S. Reynaud, Lateral Casimir-Polder force with corrugated surfaces, *J. Phys. A: Math. Theor.* **41**, 164028 (2008).
- [14] B. Döbrich, M. DeKieviet, and H. Gies, Scalar Casimir-Polder forces for uniaxial corrugations, *Phys. Rev. D* **78**, 125022 (2008).
- [15] R. Messina, D. A. R. Dalvit, P. A. Maia Neto, A. Lambrecht, and S. Reynaud, Dispersive interactions between atoms and nonplanar surfaces, *Phys. Rev. A* **80**, 022119 (2009).
- [16] G. A. Moreno, D. A. R. Dalvit, and E. Calzetta, Bragg spectroscopy for measuring Casimir-Polder interactions with Bose-Einstein condensates above corrugated surfaces, *New J. Phys.* **12**, 033009 (2010).
- [17] A. M. Contreras-Reyes, R. Guérout, P. A. Maia Neto, D. A. R. Dalvit, A. Lambrecht, and S. Reynaud, Casimir-Polder interaction between an atom and a dielectric grating, *Phys. Rev. A* **82**, 052517 (2010).
- [18] G. A. Moreno, R. Messina, D. A. R. Dalvit, A. Lambrecht, P. A. Maia Neto, and S. Reynaud, Disorder in Quantum Vacuum: Casimir-Induced Localization of Matter Waves, *Phys. Rev. Lett.* **105**, 210401 (2010).
- [19] G. Bimonte, T. Emig, and M. Kardar, Casimir-Polder interaction for gently curved surfaces, *Phys. Rev. D* **90**, 081702(R) (2014).
- [20] V. N. Marachevsky, Fluctuation potential of the interaction between a neutral atom and a diffraction grating, *Theor. Math. Phys.* **185**, 1492 (2015).
- [21] R. Bennett, Spontaneous decay rate and Casimir-Polder potential of an atom near a lithographed surface, *Phys. Rev. A* **92**, 022503 (2015).
- [22] E. C. M. Nogueira, L. Queiroz, and D. T. Alves, Peak, valley, and intermediate regimes in the lateral van der Waals force, *Phys. Rev. A* **104**, 012816 (2021).
- [23] L. Queiroz, E. C. M. Nogueira, and D. T. Alves, Regimes of the lateral van der Waals force in the presence of dielectrics, *Phys. Rev. A* **104**, 062802 (2021).
- [24] E. C. M. Nogueira, L. Queiroz, and D. T. Alves, Sign inversion in the lateral van der Waals force, *Phys. Rev. A* **105**, 062816 (2022).
- [25] L. Queiroz, E. C. M. Nogueira, and D. T. Alves, Sign inversion in the lateral van der Waals force between an anisotropic particle and a plane with a hemispherical protuberance: an exact calculation, *J. Phys. A: Math. Theor.* **56**, 115301 (2023).
- [26] C. Eberlein and R. Zietal, Force on a neutral atom near conducting microstructures, *Phys. Rev. A* **75**, 032516 (2007).
- [27] C. Eberlein and R. Zietal, Retarded Casimir-Polder force on an atom near reflecting microstructures, *Phys. Rev. A* **80**, 012504 (2009).
- [28] V. B. Bezerra, E. R. Bezerra de Mello, G. L. Klimchitskaya, V. M. Mostepanenko, and A. A. Saharian, Exact Casimir-Polder potential between a particle and an ideal metal cylindrical shell and the proximity force approximation, *Eur. Phys. J. C* **71**, 1614 (2011).
- [29] J. Rosenfeld and D. Wasan, The London force contribution to the van der Waals force between a sphere and a cylinder, *J. Colloid Interface Sci.* **47**, 27 (1974).
- [30] Y. Gu and D. Li, The van der Waals interaction between a spherical particle and a cylinder, *J. Colloid Interface Sci.* **217**, 60 (1999).
- [31] V. Kirsch, Calculation of the van der Waals force between a spherical particle and an infinite cylinder, *Adv. Colloid Interface Sci.* **104**, 311 (2003).
- [32] E. V. Blagov, G. L. Klimchitskaya, and V. M. Mostepanenko, Van der Waals interaction between microparticle and uniaxial crystal with application to hydrogen atoms and multiwall carbon nanotubes, *Phys. Rev. B* **71**, 235401 (2005).
- [33] M. Bordag, Casimir effect for a sphere and a cylinder in front of a plane and corrections to the proximity force theorem, *Phys. Rev. D* **73**, 125018 (2006).
- [34] H. Gies and K. Klingmüller, Casimir Effect for Curved Geometries: Proximity-Force-Approximation Validity Limits, *Phys. Rev. Lett.* **96**, 220401 (2006).
- [35] R. Feynman, R. Leighton, and M. Sands, *The Feynman Lectures on Physics*, Vol. II (Pearson/Addison-Wesley, Boston, 2006).
- [36] J. E. Lennard-Jones, Processes of adsorption and diffusion on solid surfaces, *Trans. Faraday Soc.* **28**, 333 (1932).
- [37] S. Y. Buhmann, *Dispersion Forces I*, Springer Tracts in Modern Physics, Vol. 247 (Springer, Berlin, 2012).
- [38] B. Amorim, P. A. D. Gonçalves, M. I. Vasilevskiy, and N. M. R. Peres, Impact of graphene on the polarizability of a neighbour nanoparticle a dyadic green's function study, *Appl. Sci.* **7**, 1158 (2017).